Available online at www.sciencedirect.com
ScienceDirect
Bioelectrochemistry 70 (2007) 296–300
Bioelectrochemistry
www.elsevier.com/locate/bioelechem

Electrochemical parameters of ethamsylate at multi-walled carbon nanotube modified glassy carbon electrodes

Sheng-Fu Wang *, Qiao Xu

Faculty of Chemistry and Material Science, Hubei University, Wuhan 430062, People's Republic of China

Received 30 July 2005; received in revised form 11 November 2005; accepted 14 December 2005
Available online 23 May 2006

Abstract

In this paper, some electrochemical parameters of ethamsylate at a multi-walled carbon nanotube modified glassy carbon electrode, such as the charge number, exchange current density, standard heterogeneous rate constant and diffusion coefficient, were measured by cyclic voltammetry, chronoamperometry and chronocoulometry. The modified electrode exhibits good promotion of the electrochemical reaction of ethamsylate and increases the standard heterogeneous rate constant of ethamsylate greatly. The differential pulse voltammetry responses of ethamsylate were linearly dependent on its concentrations in a range from 2.0×10^{-6} to 6.0×10^{-5} mol L^{-1}, with a detection limit of 4.0×10^{-7} mol L^{-1}.

Keywords: Carbon nanotube; Modified electrode; Ethamsylate; Electrochemistry; Determination

1. Introduction

Carbon nanotubes (CNTs), generated by rolling single or several layers of graphite into a seamless and hollow cylinder, can be divided into multi-walled carbon nanotubes (MWNTs) [1] and single-walled carbon nanotubes (SWNTs) [2] based on the numbers of carbon atom layers of the wall of the nanotubes. Since its discovery by Iijima [1] in 1991 using transmission electron microscopy, CNTs have been the subject of numerous investigations in chemical, physical and materials areas due to their novel structural, mechanical, electronic, and chemical properties [3,4]. Depending on their atomic structure, CNTs behave electrically as a metal or as a semiconductor [5,6]. The subtle electronic properties suggest that CNTs have the ability to promote charge-transfer reactions when used as an electrode [7–11]. Recent studies demonstrated that a CNT modified electrode can impart strong electrocatalytic activity to some important biomolecules, including cytochrome *c* [8,10], NADH [11], hydrogen peroxide [12,13], and catecholamines such as dopamine [14] and ascorbic acid [10].

Ethamsylate (ETH) (Fig. 1), as one of the catecholamines, has distinct antihemorrhagic and angioprotective properties. It restores the decreased capillary resistance, improves microcirculation, normalizes the prolonged bleeding time and enhances the adhesion of platelet. A few papers have been published for the determination of ETH in recent years [15–21], such as chemiluminescence [16,18] and spectrophotometry methods [19]. Some electrochemical methods have also been reported [15,20]. Hassan et al. proposed a potentiometric method for the determination of ETH. The detection limit of ETH was 1.0×10^{-4} mol L^{-1} [21], which was not satisfactory for the microscale analysis purposes. The detection of ETH with MWNT-modified glassy carbon electrode (GCE) has not been reported yet. In this paper, the electrochemical behavior of ETH was investigated in detail at the MWNT-modified GCE, which showed favorable electrocatalytic behavior toward the electro-oxidation of ETH, and a fast, simple and sensitive detection method for ETH was developed.

2. Experimental

2.1. Instruments

Cyclic voltammetric (CV), differential pulse voltammetry (DPV), chronoamperometric and chronocoulometric experiments were performed using a CHI660A electrochemical workstation (CH Inc., USA) coupled with a conventional three-electrode cell. The working electrode was a MWNT-

* Corresponding author. Tel.: +86 27 5086 5498.
E-mail address: wangsf@hubu.edu.cn (S.-F. Wang).

1567-5394/$ - see front matter © 2006 Elsevier B.V. All rights reserved.
doi:10.1016/j.bioelechem.2005.12.005

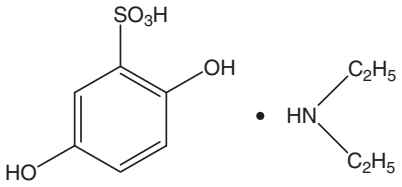

Fig. 1. Chemical structure of ethamsylate.

modified GCE or GCE, the auxiliary electrode platinum wire, and the reference electrode saturated calomel electrode (SCE). All the potentials are given against the SCE. The anodic current is assigned to be negative, and the cathodic current positive. TEM-100SX (Tokyo, Japan) was used to characterize the MWNTs.

2.2. Chemicals

Ethamsylate was obtained from Chinese Institute for the Control of Pharmaceutical and Biomedical Products (Beijing, China). Crude MWNTs were purchased from Huazhong Normal University (Wuhan, China). Crude MWNTs were ultrasonically agitated in 3 mol L^{-1} HNO_3 for 1 h and refluxed in 5 mol L^{-1} HCl for 4 h at 110 °C. After acid treatment, the samples were calcined in static air at 350 °C for about 2 h. 1 mg purified MWNTs were dispersed ultrasonically in 1 mL of *N*, *N*-dimethylformamide (DMF) to give a 1 mg mL^{-1} black suspension. Other reagents were of analytical grade. All solutions were prepared with double distilled water.

2.3. Preparation of the MWNT-modified electrode

The GCE was carefully abraded with emery paper, polished on chamois leather containing 0.05 μm alumina slurry, and then washed ultrasonically in water, ethanol and water, respectively. The cleaned GCE was coated by casting 20 μL of the black suspension of MWNT in DMF and dried in the air to remove the solvent. Then the MWNT-modified GCE was prepared.

The microscopic areas of the MWNT-modified GCE and the bare GCE were obtained by CV using 1 mmol L^{-1} $K_3Fe(CN)_6$ as a probe at different scan rates. For a reversible process, the following equation exists:

$$i_{pa} = 2.69 \times 10^5 n^{3/2} A c_0 D_R^{1/2} v^{1/2} \quad (1)$$

where i_{pa} refers to the anodic peak current. For $K_3Fe(CN)_6$, $n=1$, $D_R=7.6\times10^{-6}$ cm s^{-1}(0.1 mol L^{-1} KCl), then from the slope of the i_{pa}–$v^{1/2}$ relation, the microscopic areas can be calculated, with 0.04897 cm^2 for the bare GCE and 0.08617 cm^2 for the MWNT-modified GCE being obtained. Evidently, the modified electrode increased by nearly 76% in area.

3. Results and discussion

3.1. TEM characterization

MWNTs can be uniformly dispersed in DMF. Fig. 2 shows the structure of a MWNT pipe clearly. Some MWNTs were formed as boundless tubes because of van der Waals forces.

Fig. 2. TEM image of the purified MWNTs.

3.2. Electrochemical behavior and the electrochemical parameters of ETH at the MWNT-modified GCE

Fig. 3 shows the CVs of ETH at the MWNT-modified GCE (Fig. 3a) and the bare GCE (Fig. 3c) in 0.2 mol L^{-1} PBS (pH 5.5). As can be seen, ETH exhibits an irreversible behavior at the bare GCE with a separation of the anodic peak potential E_{pa} and the cathodic peak potential E_{pc}, ΔE_p of 652 mV at a scan rate of 0.1 V s^{-1}. However, a well-defined redox wave of ETH was observed at the MWNT-modified GCE with $\Delta E_p=68$ mV. Thus the reversibility of ETH was significantly improved. The peak current also increased greatly. The reason for the better performance of the MWNT-modified CGE may be due to the nanometer dimensions of the CNTs, the electronic structure and the topological defects present on the CNTs surfaces [22]. Meanwhile the CNTs increase the effective area of the electrode. The modified electrode has no electrochemical activity in 0.2 mol L^{-1} PBS (pH 5.5) (Fig. 3b), but the background current becomes larger, which is attributed to the fact that MWNT can increase the surface activity markedly.

The influence of scan rate on the oxidation of ETH at the MWNT-modified GCE was studied by cyclic voltammetry (Fig. 4). The redox peak current of ETH increased linearly with the square root of the scan rate in the range from 0.01 to 0.2 V s^{-1},

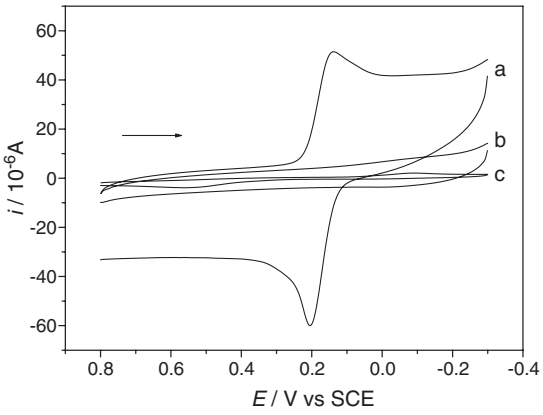

Fig. 3. Cyclic voltammograms at a MWNT-modified GCE (a) and a bare GCE (c) in the presence of 1.0×10^{-3} mol L^{-1} ETH, and a MWNT-modified GCE (b) in the absence of ETH 0.2 mol L^{-1} PBS (pH 5.5) at scan rate 0.1 V s^{-1}.

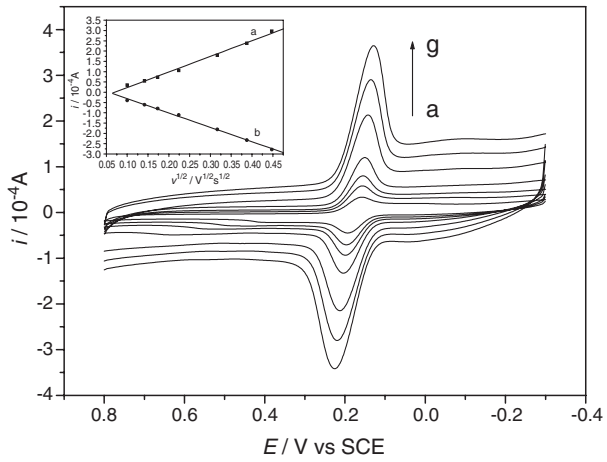

Fig. 4. Cyclic voltammograms of 1.0×10^{-3} mol L^{-1} ETH in 0.2 mol L^{-1} PBS (pH 5.5) at scan rates of (from a to g): 0.01, 0.02, 0.03, 0.05, 1.0, 1.5, 2.0 V s^{-1}. Insert: The relationship between the peak currents (a—i_{pc}, b—i_{pa}) and scan rates.

suggesting that the electrode reaction of ETH was a diffusion-controlled process.

3.3. Measurement of some electrochemical parameters of the electrode reaction

3.3.1. Charge number

The charge transfer number n is the basic parameter of an electrode reaction. Chronoamperometry and CV were used to measure the charge transfer number of ETH at the MWNT-modified GCE. The step potentials (E_2) for chronoamperometry were set near the $E_{pa/2}$. A series of currents, $I(\tau)$, at some fixed time τ were obtained from each of the step experiments. When the step potential was more positive than 0.19 V, the chronoamperometric curves became identical, indicating that the step potential entered the "mass-transfer-limited" region and the current $I(\tau)$ reached the limited current $I_d(t)$. For a fixed sampling time τ [24]

$$E = E^{0'} + \frac{RT}{nF}\ln\frac{D_R^{1/2}}{D_O^{1/2}} + \frac{RT}{nF}\ln\frac{I_d(\tau)-I(\tau)}{I(\tau)} \quad (2)$$

If $D_R = D_O$, Eq. (2) is rewritten as

$$E = E^{0'} + \frac{RT}{nF}\ln\frac{I_d(\tau)-I(\tau)}{I(\tau)}. \quad (3)$$

The charge transfer number n can be calculated based on the E vs. $\ln\frac{I_d(\tau)-I(\tau)}{I(\tau)}$ curve. Table 1 lists the results when τ were selected as 150 and 200 ms, respectively. So the charge transfer number n was about 2 and $E^{0'}$ was 0.121 V.

Table 1
Electron transfer number calculated from the chronoamperometry experiment

τ (ms)	$I_d(\tau)$ (10^{-6} A)	Slope	n	$E^{0'}$ (V)	R
150	88.89	0.0332	1.7	0.1210	0.9973
200	75.80	0.0327	1.8	0.1213	0.9944

From the CV of ETH at the MWNT-modified GCE (Fig. 3), an E_{pa} value of 0.210 V and an $E_{pa/2}$ value of 0.178 V were obtained. For a reversible system

$$|E_p - E_{p/2}| = \frac{56.5}{n}mV. \quad (4)$$

The charge transfer number n can also be calculated to be about 2.

3.3.2. The proton number

Fig. 5 shows CVs of 1.0×10^{-3} mol L^{-1} ETH in PBS at different pHs. With increasing solution pH, the anodic peak potential shifted negatively, and obeyed the following equation:

$$E_{pa}/V = 0.53 - 0.056\text{pH} \quad r = 0.9912$$

The proton number intervening in the redox process was 2, which could be calculated from the slope of the equation above. Therefore, the proposed redox mechanism for ETH can be written as follows (Fig. 6):

3.3.3. Exchange current density j^0 and standard heterogeneous rate constant k^0 at the MWNT-modified GCE, and the k^0 of ETH at bare GCE

Chronoamperometry was used to determine the exchange current density j^0 and standard heterogeneous rate constant k^0 of ETH at the MWNT-modified GCE (Fig. 7). When the step potentials were set near the formal potential, the perturbation in potential was small in size, and the reaction controlled by the electrochemical step at the modified electrode took place under almost reversible conditions. The current density and over-potential were linked by a linear j–η relation [24]:

$$j = j^0 nF\eta/RT. \quad (5)$$

For chronoamperometric experiments [23]

$$j(t) = j_{t=0}(1 - 2\lambda t^{1/2}/\pi^{1/2}) \quad (6)$$

where $j_{t=0}$ refers to the polarized current density corresponding to the overpotential η (i.e. $E_2 - E_{eq}$) without concentration

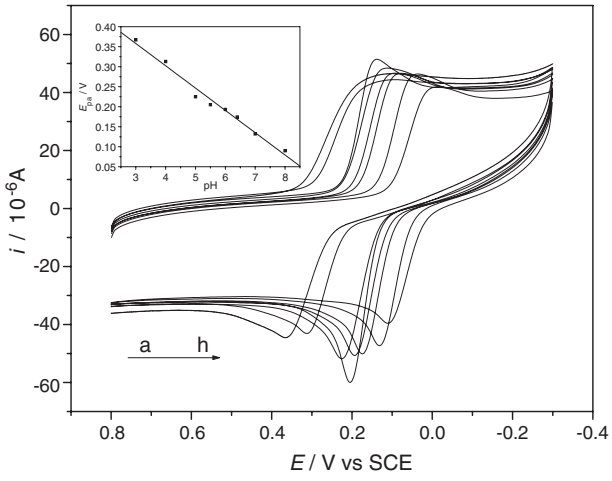

Fig. 5. Cyclic voltammograms of 1.0×10^{-3} mol L^{-1} ETH in 0.2 mol L^{-1} PBS at different pHs (a–h): 3.0, 4.0, 5.0, 5.5, 6.0, 6.4, 7.0, 8.0. Scan rate v: 0.1 V s^{-1}. Insert: Plot of E_{pa} vs. pH.

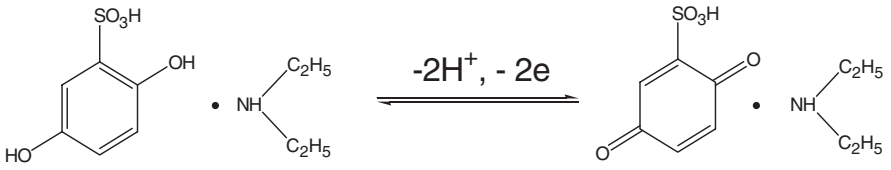

Fig. 6. Redox mechanism of ETH.

polarization. The $j_{t=0}$ can be obtained from the intercept of the $j(t)$–$t^{1/2}$ relation (Fig. 7a). Then Eq. (5) can be rewritten as

$$j_{t=0} = j^0 nF(E_2 - E_{eq})/RT. \quad (7)$$

Different $j_{t=0}$ values can be obtained with different step potentials (E_2). Fig. 7b shows the $j_{t=0}$–E_2 relation, with a correlation coefficient of 0.9999. According to the slope of 0.0112 A cm^{-2} V^{-1}, an exchange current density (j^0) of 1.43×10^{-4} A cm^{-2} was obtained. From Eq. (8) [23]

$$j^0 = nFk^0c \quad (8)$$

the standard heterogeneous rate constant of ETH at the modified electrode can be calculated, with a k^0 value of 7.4×10^{-3} cm s^{-1}.

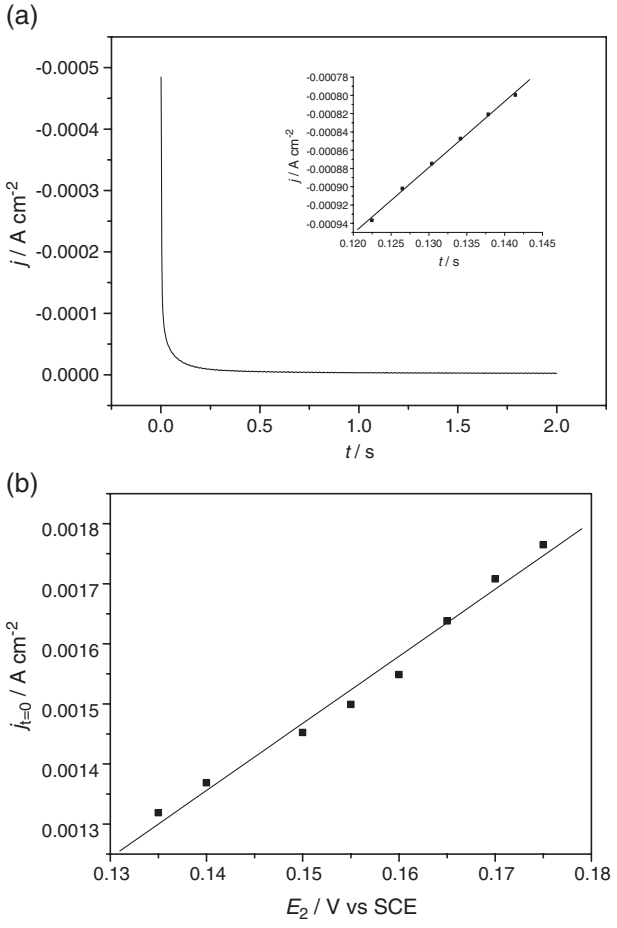

Fig. 7. (a) Chronoamperomogram for the oxidation of ETH at a MWNT-modified GCE. The inset is the plot of $j-t^{1/2}$ obtained from the data of the initial stage of (a). (b) Plot of $j_{t=0}$ against E_2 obtained from a series of potential step measurements of the MWNT-modified GCE in 0.2 mol L^{-1} PBS, pH 5.5 containing 1.0×10^{-4} mol L^{-1} ETH.

The k^0 of ETH at the bare GCE was 8.35×10^{-9} cm s^{-1} and the charge transfer coefficient α was 0.425, both of which can be calculated from the plot of E_{pa} vs. log$v$ in Eq. (10) [23].

$$E_{pa} = E^{0'} + \frac{RT}{(1-\alpha)F}\left\{0.780 + \ln\left(\frac{D_R^{1/2}}{k^0}\right) + \ln\left[\frac{(1-\alpha)nFv}{RT}\right]^{1/2}\right\}. \quad (10)$$

The standard heterogeneous rate constant k^0 is a kinetic facility of a redox couple. A system with a large k^0 will achieve equilibrium in a short time scale, but a system with small k^0 will be sluggish [23]. Compared with the k^0 value at the MWNT-modified GCE, 7.4×10^{-3} cm s^{-1}, it is clear that the modified electrode can promote the electrochemical reaction significantly.

3.3.4. The diffusion coefficient (D_R)

The diffusion coefficient of ETH was determined at the MWNT-modified GCE using chronocoulometry based on the following equation [24]:

$$Q = \frac{2nFAD_R^{1/2}c_0t^{1/2}}{\pi^{1/2}} + Q_{dl} + nFA\Gamma_o \quad (9)$$

The potential step was from 0 to 0.3 V (Fig. 8), the curve of Q vs. $t^{1/2}$ with a correlation coefficient of 0.9963. Based on the slope of Q–$t^{1/2}$ curve, 0.233 μC s$^{-1/2}$, the diffusion coefficient (D_R) of ETH was estimated as 6.15×10^{-6} cm^2 s^{-1}.

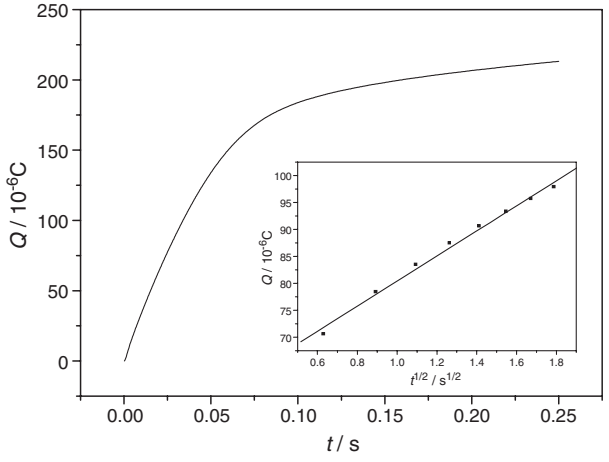

Fig. 8. Plot of Q–t curve of the MWNT-modified GCE in 0.2 mol L^{-1} PBS, pH 5.5 containing 1.0×10^{-3} mol L^{-1} ETH. Insert: Plot of Q–$t^{1/2}$ curve of the modified GCE in 0.2 mol L^{-1} PBS, pH 5.5 containing 1.0×10^{-3} mol L^{-1} ETH.

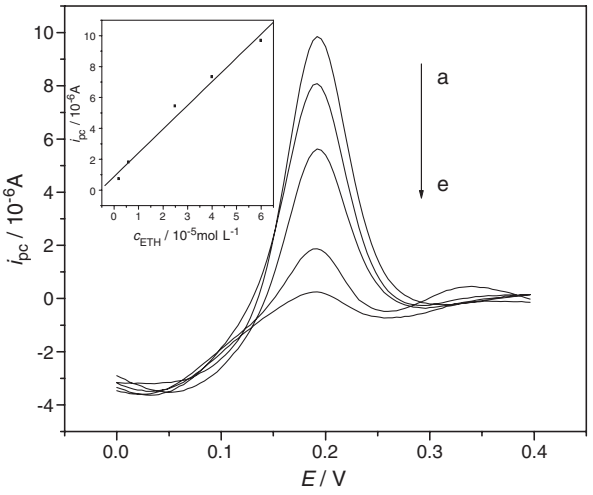

Fig. 9. DPV curves of a MWNT-modified GCE in ETH solution at different concentrations a, 6.0×10^{-5}; b, 4.0×10^{-5}; c, 2.5×10^{-5}; d, 6.0×10^{-6}; e, 2.0×10^{-6} mol L^{-1}. Insert: Plots of the peak current against the concentration of ETH.

3.4. Determination of ETH at the MWNT-modified GCE

The calibration curve for ETH in pH 5.5 PBS was measured by DPV. Fig. 9 shows the DPV curves of ETH at the MWNT-modified GCE at various concentrations. The peak current increased linearly with increment of ETH in the range from 2.0×10^{-6} to 6.0×10^{-5} mol L^{-1}. The linear regression equation was expressed as $i/10^{-6}$ A$=0.530+0.147c_{ETH}/10^{-6}$ mol L^{-1}, $r=0.9911$, and the detection limit (three times the signal blank/slope) was 4.0×10^{-7} mol L^{-1}. The RSD of 1.0×10^{-4} mol L^{-1}, ethamsylate signal is 2.5% ($n=10$).

4. Conclusion

The electrochemistry of ETH was studied by several electrochemical methods at a glassy carbon electrode modified with MWNTs. A pair of well-defined redox waves was obtained. The electrochemical behavior of ETH at the MWNT-modified GCE is a diffusion-controlled process involving two charges accompanied by a transfer of two protons. Some electrochemical parameters of ETH electro-oxidation were measured. The MWNT-modified GCE showed promising promotion of the electrochemical reaction of ETH. The standard heterogeneous rate constant k^0 is increased by an order of magnitude. The peak currents of DPV increased linearly with the concentrations of ETH in the range from 2.0×10^{-6} to 6.0×10^{-5} mol L^{-1} and the detection limit was 4.0×10^{-7} mol L^{-1}.

Acknowledgement

The work was supported by the Natural Foundation of Hubei province of PR China (2005ABA063).

References

[1] S. Iijima, Helical microtubules of graphitic carbon, Nature 354 (1991) 56–58.
[2] S. Iijima, T. Ichihashi, Single-shell carbon nanotubes of 1-nm diameter, Nature 363 (1993) 603–605.
[3] P.M. Ajayan, Nanotubes from carbon, Chem. Rev. 99 (1999) 1787–1800.
[4] T.W. Odom, J.L. Huang, P. Kim, C.M. Lieber, Atomic structure and electronic properties of single-walled carbon nanotubes, Nature 391 (1998) 62–64.
[5] J.W. Jang, D.K. Lee, C.E. Lee, T.J. Lee, C.J. Lee, S.J. Noh, Metallic conductivity in bamboo-shaped multiwalled carbon nanotubes, Solid State Commun. 122 (2002) 619–622.
[6] D. Tekleab, R. Czerw, D.L. Carroll, P.M. Ajayan, Electronic structure of kinked multiwalled carbon nanotubes, Appl. Phys. Lett. 76 (2000) 3594–3596.
[7] J.M. Nugent, K.S.V. Santhanam, A. Rubio, P.M. Ajayan, Fast electron transfer kinetics on multiwalled carbon nanotube microbundle electrodes, Nano Lett. 1 (2001) 87–91.
[8] J.J. Davis, R.J. Coles, H. Allen, O. Hill, Protein electrochemistry at carbon nanotube electrodes, J. Electroanal. Chem. 440 (1997) 279–282.
[9] H. Luo, Z. Shi, N. Li, Z. Gu, Q. Zhuang, Investigation of the electrochemical and electrocatalytic behavior of single-wall carbon nanotube film on a glassy carbon electrode, Anal. Chem. 73 (2001) 915–920.
[10] J. Wang, M. Li, Z. Shi, N. Li, Z. Gu, Direct electrochemistry of cytochrome *c* at a glassy carbon electrode modified with single-wall carbon nanotubes, Anal. Chem. 74 (2002) 1993–1997.
[11] M. Musameh, J. Wang, A. Merkoci, Y. Lin, Low-potential stable NADH detection at carbon-nanotube-modified glassy carbon electrodes, Electrochem. Comm. 4 (2002) 743–746.
[12] J. Wang, M. Musameh, Y. Lin, Solubilization of carbon nanotubes by nafion toward the preparation of amperometric biosensors, J. Am. Chem. Soc. 125 (2003) 2408–2409.
[13] J. Wang, M. Musameh, Carbon nanotube/teflon composite electrochemical sensors and biosensors, Anal. Chem. 75 (2003) 2075–2079.
[14] K.B. Wu, J.J. Fei, S.H. Hu, Simultaneous determination of dopamine and serotonin on a glassy carbon electrode coated with a film of carbon nanotubes, Anal. Biochem. 318 (2003) 100–106.
[15] X.H. Zhang, S.F. Wang, Determination of ethamsylate in the presence of catecholamines using 4-amino-2-mercaptopyrimidine self-assembled monolayer gold electrode, Sens. Actuators, B, Chem. 104 (2005) 29–34.
[16] F.Z. Yang, C. Zhang, W.R.G. Baeyens, X.R. Zhang, Determination of ethamsylate in pharmaceutical preparations based on an auto-oxidation chemiluminescence reaction, J. Pharm. Biomed. Anal. 30 (2002) 473–478.
[17] J.Q. Chen, J.F. Song, L.F. Chen, Determination of ethamsylate in pharmaceutical preparations by irreversible biamperometry, Microchem. J. 80 (2005) 65–70.
[18] J.X. Du, Y.H. Li, Y. Tang, J.R. Lu, Flow injection chemiluminescence determination of ethamsylate based on permanganate oxidation, Anal. Lett. 35 (2002) 463–465.
[19] Z.C. Xu, X.Y. Li, J. Shi, X.J. Yao, A.Z. Liu, Z.S. He, Determination of ethamsylate by UV spectrophotometry, Chin. J. Anal. Chem. 22 (1994) 420–421.
[20] S.S.M. Hassan, R.M. El-Bahnasawy, N.M. Rizk, Determination of ETH with potentiometric method, MiKrochim. Acta 126 (1997) 217–219.
[21] G.J. Yang, L.T. Jin, Z.Z. Leng, Determination of microscale ethamsylate on carbon paste electrode with adsorptive voltammetry, Chin. J. Pharm. Anal. 18 (1998) 311–313.
[22] P.J. Britto, K.S.V. Santhanam, A. Rubio, J.A. Alonso, P.M. Ajayan, Improved charge transfer at carbon nanotube electrodes, Adv. Mater. 11 (1999) 154–157.
[23] A.J. Bard, L.R. Faulkner, Electrochemical Methods, second ed., Wiley, New York, 1980 chapter 3.
[24] A.J. Bard, L.R. Faulkner, Electrochemical Methods, second ed., Wiley, New York, 1980 chapter 5.